Biochemical Journal (2017) **474** 179–194
DOI: 10.1042/BCJ20160876

PORTLAND PRESS

Research Article

Kinetic and thermodynamic studies of the interaction between activating and inhibitory Ly49 natural killer receptors and MHC class I molecules

Pablo N. Romasanta[1], Lucrecia M. Curto[2], María B. Sarratea[1], Sofía Noli Truant[1], María B. Antonoglou[1], María J. Fernández Lynch[1], José M. Delfino[2], Roy A. Mariuzza[3], Marisa M. Fernández[1] and Emilio L. Malchiodi[1]

[1]Universidad de Buenos Aires, Facultad de Farmacia y Bioquímica, Cátedra de Inmunología and Instituto de Estudios de la Inmunidad Humoral (IDEHU), UBA-CONICET, Buenos Aires, Argentina; [2]Universidad de Buenos Aires, Facultad de Farmacia y Bioquímica, Departamento de Química Biológica and Instituto de Química y Fisicoquímica Biológica (IQUIFIB), UBA-CONICET, Buenos Aires, Argentina; and [3]University of Maryland Institute for Bioscience and Biotechnology Research, W. M. Keck Laboratory for Structural Biology, Rockville, MD, USA.

Correspondence: Emilio L. Malchiodi (emalchio@ffyb.uba.ar)

Natural killer (NK) cells are lymphocytes of the innate immune system that eliminate virally infected or malignantly transformed cells. NK cell function is regulated by diverse surface receptors that are both activating and inhibitory. Among them, the homodimeric Ly49 receptors control NK cell cytotoxicity by sensing major histocompatibility complex class I molecules (MHC-I) on target cells. Although crystal structures have been reported for Ly49/MHC-I complexes, the underlying binding mechanism has not been elucidated. Accordingly, we carried out thermodynamic and kinetic experiments on the interaction of four NK Ly49 receptors (Ly49G, Ly49H, Ly49I and Ly49P) with two MHC-I ligands (H-2D^d and H-2D^k). These Ly49s embrace the structural and functional diversity of the highly polymorphic Ly49 family. Combining surface plasmon resonance, fluorescence anisotropy and far-UV circular dichroism (CD), we determined that the best model to describe both inhibitory and activating Ly49/MHC-I interactions is one in which the two MHC-I binding sites of the Ly49 homodimer present similar binding constants for the two sites ($\sim 10^6$ M^{-1}) with a slightly positive co-operativity in some cases, and without far-UV CD observable conformational changes. Furthermore, Ly49/MHC-I interactions are diffusion-controlled and enthalpy-driven. These features stand in marked contrast with the activation-controlled and entropy-driven interaction of Ly49s with the viral immunoevasin m157, which is characterized by strong positive co-operativity and conformational selection. These differences are explained by the distinct structures of Ly49/MHC-I and Ly49/m157 complexes. Moreover, they reflect the opposing roles of NK cells to rapidly scan for virally infected cells and of viruses to escape detection using immunoevasins such as m157.

Introduction

Natural killer (NK) cells are essential components of the innate immune response against viruses and tumors [1–4]. They not only eliminate virally infected or malignantly transformed cells via their cytolytic abilities, but also produce cytokines that modulate immune responses and maintain tissue homeostasis. To perform these functions, NK cells express diverse activating and inhibitory receptors that act in concert to regulate their activities [5,6]. The dominant signal received by an NK cell is inhibitory, provided by the interaction of its receptors with normal levels of major histocompatibility complex class I molecules (MHC-I). If MHC-I expression is reduced by viral infections or tumorigenic processes, this inhibitory signal is attenuated and the NK cell undergoes activation. As a consequence, cells with reduced MHC-I expression become subject to lysis by NK cells [1–4].

Received: 21 September 2016
Revised: 1 November 2016
Accepted: 9 November 2016

Accepted Manuscript online: 9 November 2016
Version of Record published: 22 December 2016

PORTLAND PRESS

Biochemical Journal (2017) **474** 179–194
DOI: 10.1042/BCJ20160876

Several receptor families on primate and rodent NK cells are responsible for monitoring MHC-I expression on surrounding cells [7]. These include the killer immunoglobulin-like receptors (KIRs) in humans and the Ly49 family in rodents. The mouse Ly49 family comprises at least 23 members (Ly49A–W), along with multiple allelic variants [8,9]. Although most Ly49s inhibit NK cell-mediated cytolysis upon recognizing MHC-I ligands, some are activating [9,10]. Inhibitory Ly49s transmit signals via immunoreceptor tyrosine-based inhibitory motifs (ITIMs) located in their cytoplasmic domains. Activating Ly49s instead use the associated signaling adaptor DAP12, which contains immunoreceptor tyrosine-based activating motifs (ITAMs). Crucial roles for Ly49 receptors in antiviral immunity have also been demonstrated. For example, the m157 glycoprotein of mouse cytomegalovirus (MCMV) was shown to bind directly to an inhibitory Ly49 (Ly49I) in a susceptible mouse strain (129/J) and to an activating Ly49 (Ly49H) in a resistant one (C57BL/6) [11,12]. These interactions by m157, a viral immunoevasin and MHC-I mimic, govern the spread of MCMV and its evolutionary survival [13,14].

Although functional Ly49 genes are not found in humans, the KIR family of NK cell receptors probably mediates the same immune functions. Like Ly49, KIR genes show remarkable genetic diversity within the population and encode both inhibitory and activating receptors that are expressed on subsets of NK cells. Although HLA class I ligands have been identified for most of the inhibitory KIRs, activating KIRs appear not to bind HLA class I or do so with low affinity [6].

Considerable structural information is available for Ly49 receptors in unbound form and in complex with MHC-I and viral ligands [7]. Ly49s are homodimeric type II transmembrane glycoproteins (N-terminus inside the NK cell), with each chain containing a C-type lectin-like domain, known as the natural killer receptor domain (NKD). Each NKD of the Ly49 homodimer is linked by a helical stalk of ~70 residues to the transmembrane and cytoplasmic domains. Crystal structures have been determined for Ly49A NKD in complex with H-2D^{d} [15], Ly49C NKD bound to H-2K^{b} [16,17], Ly49C NKD [17], Ly49L NKD [18], Ly49L NKD with the stalk region [18] and Ly49H bound to the MCMV immunoevasin m157 [19].

These studies have revealed that Ly49 receptors can adopt two distinct conformations: (1) a backfolded conformation in which the NKDs of the Ly49 homodimer are backfolded onto the stalk region (Figure 1A) and (2) an extended conformation in which the NKDs project away from the stalk (Figure 1B). These two conformations mediate MHC-I binding in *trans* and *cis*, respectively [18]. Moreover, Ly49 receptors are capable of switching between backfolded and extended conformations [18,20].

The backfolded conformation enables Ly49 to engage two MHC-I molecules in *trans*, with Ly49 on the NK cell and MHC-I on an opposing target cell (Figure 1C). On the other hand, the extended conformation permits

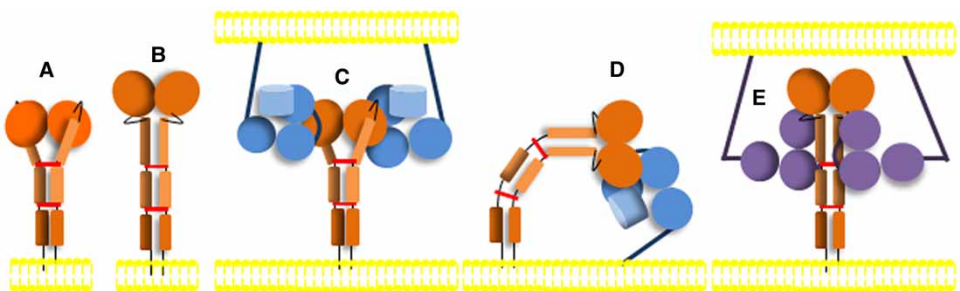

Figure 1. Conformations adopted by Ly49 receptors and interaction with MHC-I and the cytomegalovirus immunoevasin m157.

(**A**) The backfolded conformation of Ly49 on the NK cell membrane (*bottom*). The NKDs of the Ly49 homodimer (*orange ovals*) are backfolded onto the α-helical stalk region (*orange rectangles*) with interchain disulfides drawn as *red bars* [18]. (**B**) The extended conformation of Ly49 in which the NKDs extend away from the stalk. (**C**) Ly49 in the backfolded conformation binding in *trans* to two MHC-I molecules (*blue*) exposed on the target cell membrane (*top*) [18]. The interaction with MHC-I is mediated by the NKDs. (**D**) Ly49 in the extended conformation binding in *cis* to one MHC-I molecule on the same NK cell. (**E**) Ly49 in the extended conformation binding in *trans* to two m157 molecules (*purple*) on the target cell. The interaction with m157 is mediated by the Ly49 stalk region, not the NKDs [19]. The Ly49/m157 interaction is characterized by strong positive co-operativity and conformational selection, such that the second m157 binds the Ly49 homodimer with a 1000-fold higher sequential constant than the first m157 (~10^{8} versus ~10^{5} M^{-1}) [20].

Biochemical Journal (2017) **474** 179–194
DOI: 10.1042/BCJ20160876

Ly49 to bind one MHC-I molecule in *cis*, with Ly49 and MHC-I on the same NK cell (Figure 1D). In contrast with MHC-I, the MCMV immunoevasin m157 recognizes the stalk region of Ly49 rather than the NKDs, such that two m157 molecules bind the Ly49 dimer (Figure 1E) [19]. This recognition mode is only possible with Ly49 in the extended form, the conformation that engages MHC-I in *cis* (Figure 1D).

Recently, we showed that the Ly49/m157 interaction involves a conformational selection mechanism in which only the extended conformation of Ly49 can bind a first m157 ligand, followed by binding of a second m157 [20]. The interaction is characterized by strong positive co-operativity, whereby the second m157 binds the Ly49 homodimer 1000-fold more tightly than the first. The rate-limiting step in the overall mechanism is a conformational transition in Ly49 from its backfolded to extended form. In the present study, we used surface plasmon resonance (SPR), fluorescence anisotropy (FA) and circular dichroism (CD) to dissect the Ly49/MHC-I-binding mechanism for both inhibitory and activating Ly49 receptors. The combined thermodynamic and kinetic measurements revealed major differences in the way Ly49 receptors engage MHC-I compared with m157. Moreover, these differences may be understood in terms of the distinct structures of Ly49/MHC-I and Ly49/m157 complexes, as well as the distinct biological roles of Ly49/MHC-I and Ly49/m157 interactions.

Materials and methods

Protein expression and purification

The extracellular portion of Ly49H from mouse strain C57BL/6 (residues 88–266) comprising the NKD and most of the stalk region was produced by *in vitro* folding from *Escherichia coli* inclusion bodies, as we described recently [20]. Dimers were recovered after purification. The extracellular portions of Ly49I from mouse strain 129/J (residues 88–269), Ly49G from mouse strain Balb/c (residues 88-267) and Ly49P from mouse strain MA/My (residues 88–263) were prepared similarly. Biotinylated versions of these Ly49s (Ly49HAvi, Ly49IAvi, Ly49GAvi and Ly49PAvi) were produced as described recently [20]. All recombinant proteins were characterized by mass spectrometry, CD, tryptophan emission fluorescence and size exclusion chromatography.

Soluble H-2D^d and H-2D^k MHC-I molecules loaded with selected peptides were prepared by *in vitro* folding. The peptide used for H-2D^d (RGPGRAFVTI) is derived from HIV gp120 glycoprotein [21]. For H-2D^k, two peptides were chosen. One peptide (RRLGRTLLL) corresponds to the C-terminus of the polyoma virus MT protein [22]. The other peptide (DRSLRLPAR) was selected from a MCMV Smith strain open reading frames database [23] utilizing the online server NetMHC 3.0 (http://www.cbs.dtu.dk/services/NetMHC-3.0/) [24]. This MCMV peptide, which belongs to the immunogenic protein m107, was predicted to bind H-2D^k with high affinity. For production of recombinant H-2D^d and H-2D^k, H-2D heavy chains and β_2-microglobulin were separately expressed as inclusion bodies in *E. coli* BL21(DE3) and solubilized in 6 M guanidine. *In vitro* folding was carried out as described previously [21] by dilution of a mixture of H-2D heavy chains, β_2-microglobulin and peptides. Correctly folded HIV/H-2D^d, MT/H-2D^k and MCMV/H-2D^k complexes were purified using a Superdex 200 HR column (GE Healthcare).

Far-UV CD

Far-UV spectra (190–250 nm) were recorded as described recently [20]. Protein concentrations were 2 μM for Ly49 receptors and 2 or 4 μM for H-2D ligands. To study conformational changes in Ly49s, the receptors were incubated for 3 min at room temperature with the H-2D ligand at Ly49:H-2D molar ratios of 1:1 and 1:2 prior to data collection. The experimental spectrum of the mixtures was compared with the algebraic sum of the spectra for the unbound components. To calculate molar ellipticity, data were normalized by the mean weight of an amino acid in each mixture. Data analysis was carried out using the GraphPad Prism software and Microsoft Excel.

SPR binding assays

The interaction of Ly49Avi receptors with H-2D^d or H-2D^k was measured by SPR. All binding assays were performed at 5, 10, 15, 25 and 30°C using a BIAcore T100 biosensor as described recently [20]. Biotin-tagged Ly49HAvi, Ly49IAvi, Ly49GAvi or Ly49PAvi was directionally coupled to a CM5 chip onto which streptavidin had been previously immobilized via primary amine groups with an Amine Coupling kit (GE Healthcare). One or two hundred response units (RUs) of each Ly49Avi receptor were immobilized on the chip. The concentration range used was 0–5 μM for H-2D^d and 0–15 μM for H-2D^k.

Biochemical Journal (2017) **474** 179–194
DOI: 10.1042/BCJ20160876

For equilibrium analyses, response levels at the maximum RU value for each concentration of ligand were plotted against the H-2D^d or H-2D^k concentration, and the Hill equation was fitted to the data points [25]. For kinetic analyses, association and dissociation data were analyzed together and fitted globally [26,27] according to the differential equations for a model considering sequential ligand binding, using numerical integration with the software BIAevaluation 4.1 (GE Healthcare) and the Levenberg–Marquardt algorithm [28]. For numerical integration, a fifth-order Runge-Kutta–Fehlberg method was applied [28]. For activation energy analyses, kinetic rate constants obtained using a two-site model were plotted against the inverse of temperature to construct Eyring graphs according to the classical transition state theory for absolute reaction rates [29].

Fluorescence anisotropy binding assays

Ly49 receptors were labeled with fluorescein isothiocyanate (FITC) as described recently [20]. Ly49-FITC (1 μM) was titrated with different concentrations of H-2D^d or H-2D^k (0–6 μM), and FA was measured in a Jasco FP-6500 spectrofluorometer at 25°C when the interaction had reached equilibrium after 3 min equilibration in darkness at room temperature [20]. A plot of anisotropy versus H-2D^d or H-2D^k concentration was constructed. An equation that links anisotropy (r) with total (free plus bound) H-2D^d or H-2D^k concentration was fitted to the experimental data (Supplementary Equations S6–S9). Nonlinear least-square data fitting was performed using the Mathematica 9 software (Wolfram Research) utilizing the Levenberg–Marquardt algorithm [28].

Results

Recombinant Ly49 proteins

The extracellular portions of Ly49H, Ly49I, Ly49G and Ly49P (residues 88–266, 88–269, 88–267 and 88–263, respectively) were expressed as disulfide-linked homodimers after *in vitro* folding from bacterial inclusion bodies [18,20]. The recombinant proteins comprised the entire NKD and most of the helical stalk region, including Cys100, which, in the crystal structure of Ly49L [18], connects two Ly49 monomers through a disulfide bridge (Cys100–Cys100) between stalk regions.

Maximum response SPR analysis

To study the interaction between Ly49 receptors and MHC-I ligands, SPR experiments were performed for the pairs Ly49H/H-2D^d, Ly49I/H-2D^d and Ly49G/H-2D^k. H-2D^d was loaded with a peptide (RGPGRAFVTI) derived from human immunodeficiency virus (HIV) gp120 glycoprotein [21]. H-2D^k was loaded with a peptide (RRLGRTLLL) corresponding to the C-terminus of middle T (MT) polyoma virus protein [22]. Ly49Avi constructions were specifically biotinylated at their N-termini and directionally immobilized on a biosensor surface previously saturated with streptavidin. Thus, Ly49 molecules were uniformly oriented with their binding sites fully exposed. Different H-2D^d (0–5 μM) or H-2D^k (0–15 μM) concentrations were injected over the immobilized Ly49s, and sensograms were registered. Figure 2 shows a plot of the maximum response in RU obtained for each MHC-I concentration for the pairs Ly49H/H-2D^d, Ly49I/H-2D^d and Ly49G/H-2D^k at 25°C. These plots were constructed from plots of initial rates and are not steady-state binding data. The response RU values are based on the maximum response after a certain fixed contact time. We were not able to reach steady state because this would require extremely high amounts of MHC-I recombinant protein. Fitting of the Hill equation [25] (Supplementary Information) to the experimental points yielded an nH coefficient of 1.2 ± 0.2 for the Ly49H/H-2D^d pair, 1.5 ± 0.3 for the Ly49I/H-2D^d pair and 1.0 ± 0.3 for the Ly49G/H-2D^k pair. $K_{0.5}$ fitted values were 2.0 ± 0.4, 3.7 ± 0.7 and 1.4 ± 0.9 μM, respectively. In the case of Ly49G/H-2D^k, we did not observe a sigmoidal tendency of the experimental points. However, in the cases of Ly49H/H-2D^d and Ly49I/H-2D^d, the plotted line shows a slight inflection at low concentrations of H-2D^d, and the Hill coefficients (1.2 ± 0.2 and 1.5 ± 0.3, respectively) seem to confirm this trend. Importantly, this situation differs considerably from that described by Romasanta et al. [20], where strong positive co-operativity was observed, with pronounced sigmoidal tendencies and Hill values of 1.7 ± 0.1 for Ly49H/m157 and 1.9 ± 0.2 for Ly49I/m157 [20]. Considering that the Ly49 homodimer possesses two possible binding sites for MHC-I [16–18], the simplest model that might explain the Ly49/MHC-I interaction is one in which both sites are identical and independent in the three cases, at least for the Ly49G/H-2D^k pair. Certainly, if a slightly positive co-operativity does occur, it is not manifested to the same extent as it is for the Ly49/m157 interaction.

Biochemical Journal (2017) **474** 179–194
DOI: 10.1042/BCJ20160876

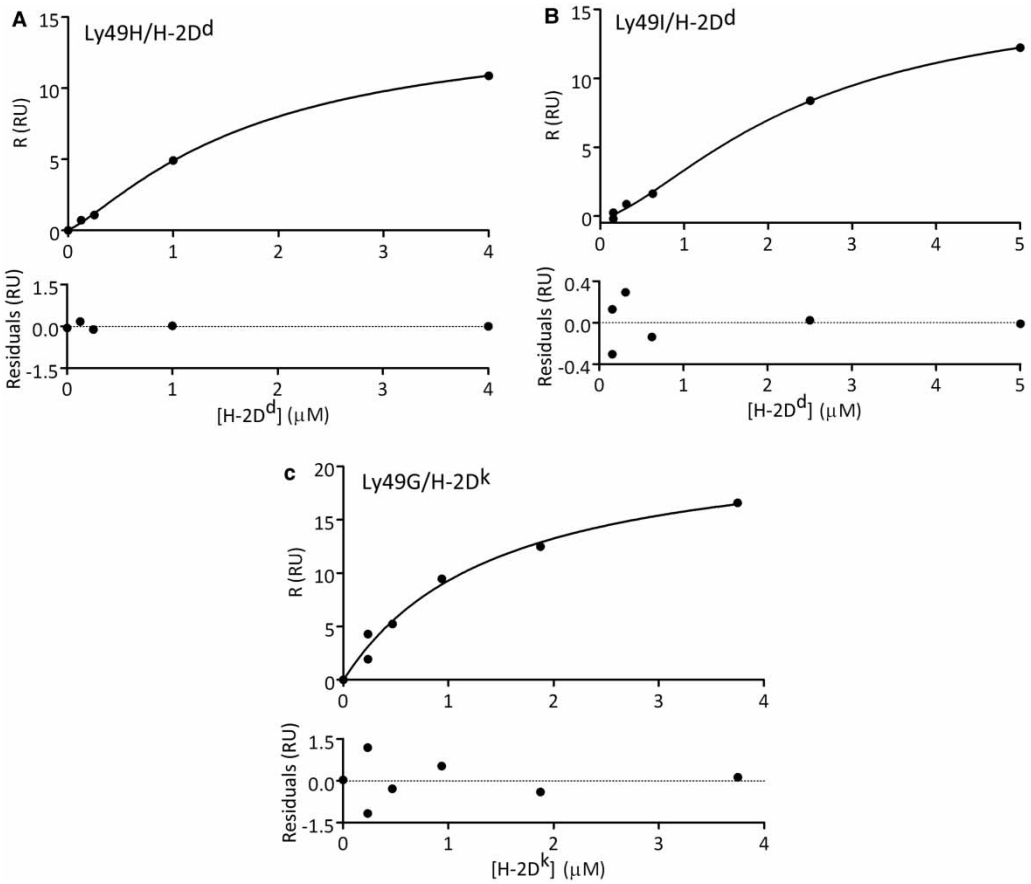

Figure 2. SPR equilibrium analysis.

Plots of the maximum response (*R*) in RU obtained at each MHC-I total concentration assayed by injection over immobilized Ly49H (**A**), Ly49I (**B**) and Ly49G (**C**) at 25°C. The curves describe the fitting to the Hill equation. The *nH* coefficient obtained for the Ly49H/H-2D^d pair is 1.2 ± 0.2, for the Ly49I/H-2D^d pair is 1.5 ± 0.3 and for the Ly49G/H-2D^k pair is 1.0 ± 0.3. Residual errors are indicated below each panel.

FA equilibrium analysis

To further characterize Ly49/MHC-I interactions, we performed solution FA assays under equilibrium binding conditions. FITC-labeled Ly49s were incubated with different concentrations of H-2D^d or H-2D^k. Figure 3 shows FA as a function of H-2D total molar concentration. Ly49H-FITC (1 μM) and Ly49I-FITC (1 μM) were titrated with H-2D^d, and Ly49G-FITC (1 μM) was titrated with H-2D^k. FA was measured after the interaction had reached equilibrium. It was possible to establish a model that accounts for the experimental data and calculate affinity constants for each H-2D-binding site of the Ly49 homodimer [30,31]. Reaction schemes and equations are provided in Supplementary Information. The estimated global constants *KG*1 and *KG*2, the sequential macroscopic constants *Ks*1 and *Ks*2 and the microscopic constants k and k' for each binding site of Ly49H, Ly49I and Ly49G are presented in Table 1. In all cases, both binding sites showed microscopic constants of the same order ($\sim 10^6$ M^{-1}). However, for Ly49H/H-2D^d and Ly49I/H-2D^d, $k' > k$ in concordance with the nH coefficients obtained with the SPR analysis. These facts lead to the conclusion that a slight positive cooperativity process may be taking place. For the Ly49G/ H-2D^k pair, this result indicates that the two MHC-I binding sites of Ly49 receptors are identical and independent [30,32,33], in agreement with SPR analysis.

Far-UV CD equilibrium analysis

To compare the different models proposed for Ly49/m157 [20] and Ly49/MHC-I interactions, we conducted far-UV CD assays. Figure 4 shows the far-UV CD spectra of the free forms of Ly49H, Ly49I and Ly49G, and

Biochemical Journal (2017) **474** 179–194
DOI: 10.1042/BCJ20160876

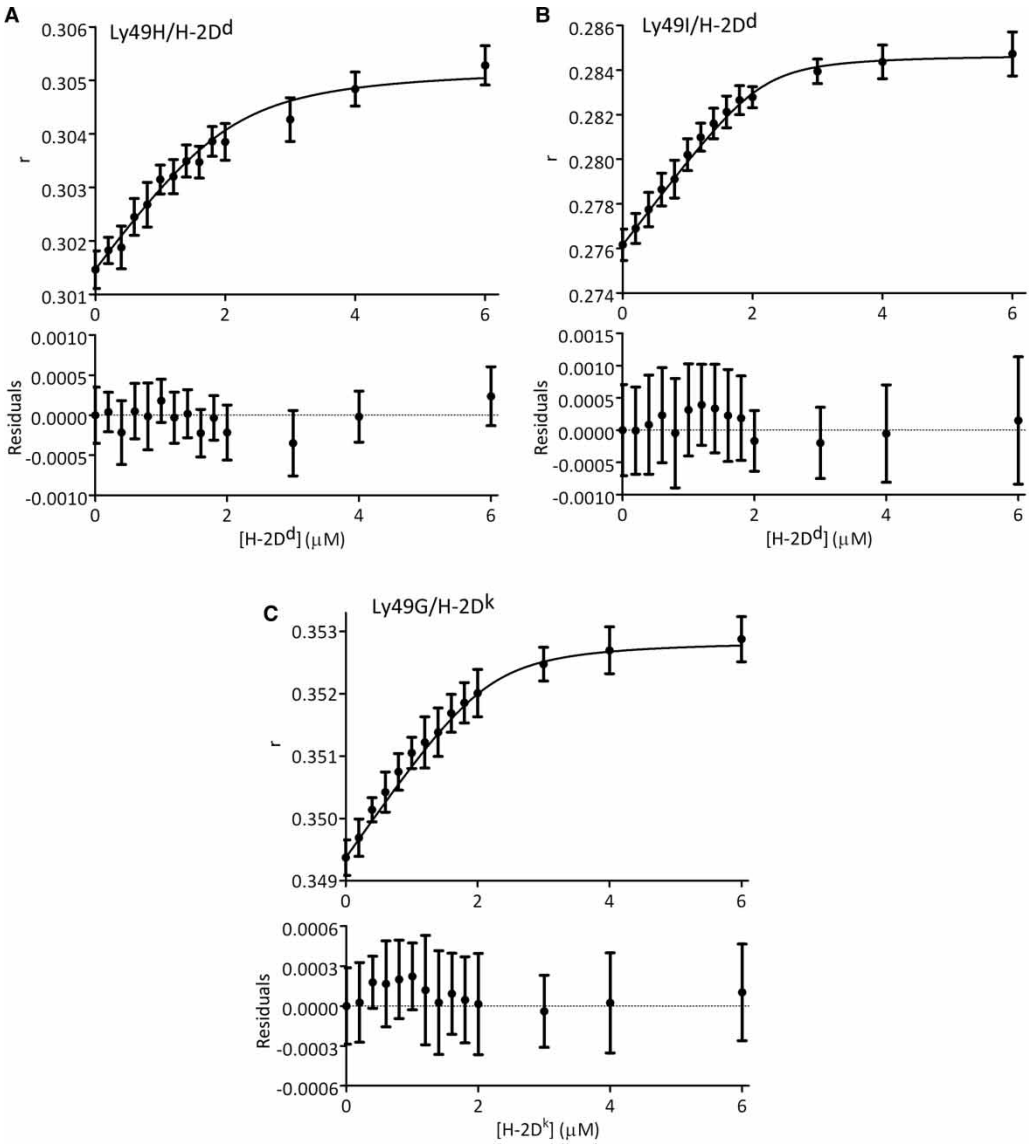

Figure 3. Equilibrium fluorescence anisotropy (*r*) as a function of MHC-I concentration.

Ly49H-FITC (**A**), Ly49I-FITC (**B**) and Ly49G-FITC (**C**) at the 1 μM concentration were titrated at 25°C with MHC-I, and FA was measured after the interaction had reached equilibrium. The curves describe the fitting to an equation that links the anisotropy (*r*) to the total MHC-I molar concentration. The constants (*KG*1, *KG*2, *Ks*1, *Ks*2, *k* and *k*′) are given in Table 1. Error bars represent SD.

Table 1 Ly49H/H-2D^d, Ly49I/H-2D^d and Ly49G/H-2D^k binding constants estimated from the FA data after fitting a model with two independent sites

*KG*1 and *KG*2, global macroscopic constants; *Ks*1 and *Ks*2, sequential macroscopic constants; *k* and *k*′, microscopic constants.

	***KG*1 × 10^6 (M^{-1})**	***KG*2 × 10^{13} (M^{-2})**	***Ks*1 × 10^6 (M^{-1})**	***Ks*2 × 10^6 (M^{-1})**	***k* × 10^6 (M^{-1})**	***k*′ × 10^6 (M^{-1})**
Ly49H/H-2D^d	5 ± 3	1.0 ± 0.4	5 ± 3	2 ± 1	3 ± 1	4 ± 3
Ly49I/H-2D^d	5 ± 3	4 ± 1	5 ± 3	8 ± 7	3 ± 2	20 ± 10
Ly49G/H-2D^k	5 ± 3	2.1 ± 0.7	5 ± 3	5 ± 4	10 ± 6	9 ± 8

Biochemical Journal (2017) **474** 179–194
DOI: 10.1042/BCJ20160876

those obtained after incubation of Ly49 and MHC-I at different molar ratios, compared with the algebraic sum of free Ly49 and free MHC-I spectra. Preincubated proteins presented the same form and intensity (molar ellipticity, [θ]) as the theoretical sum of the spectra. These results contrast with the co-incubation of Ly49 and m157 proteins, which produced lower signal intensity than that resulting from the algebraic addition of the individual spectra, indicating a conformational change in Ly49 upon binding the viral ligand [20]. Moreover, unlike the Ly49/m157 interaction [20], there is no evidence that MHC-I binding is associated with fixation of Ly49 in the extended conformation. Indeed, interchange between backfolded and extended conformations may still be possible while MHC-I is bound to Ly49. Alternatively, Ly49 may remain in the backfolded conformation, which is the most stable form when bound to MHC-I [18]. Collectively, these results reveal fundamental differences between Ly49 binding to endogenous MHC-I ligands versus the MCMV immunoevasin m157 [20].

Kinetic SPR analysis

Considering that Ly49H and Ly49I homodimers may present a slight cooperativity process when binding MHC-I, that Ly49G homodimers have two identical and independent binding sites for MHC-I — as demonstrated by SPR and FA equilibrium experiments —, and that there is no evidence of conformational change in Ly49 when interacting with MHC-I — as shown by far-UV CD studies —, the most plausible molecular mechanism for these interactions is a sequential 1:1 binding of the two H-2D ligands to Ly49. The first event of the molecular mechanism is the encounter of a Ly49 dimer molecule (in equilibrium between its backfolded and its extended state) with one MHC-I ligand to form the first bimolecular complex Ly49/MHC-I. This complex can fluctuate between Ly49 backfolded and extended forms. Then, a second MHC-I molecule joins the Ly49/MHC-I complex, consolidating a trimolecular complex backfolded Ly49/$(MHC\text{-}I)_2$. Since Ly49 is a symmetric homodimer, it is considered that the microscopic species MHC-I/Ly49 (MHC-I attached to

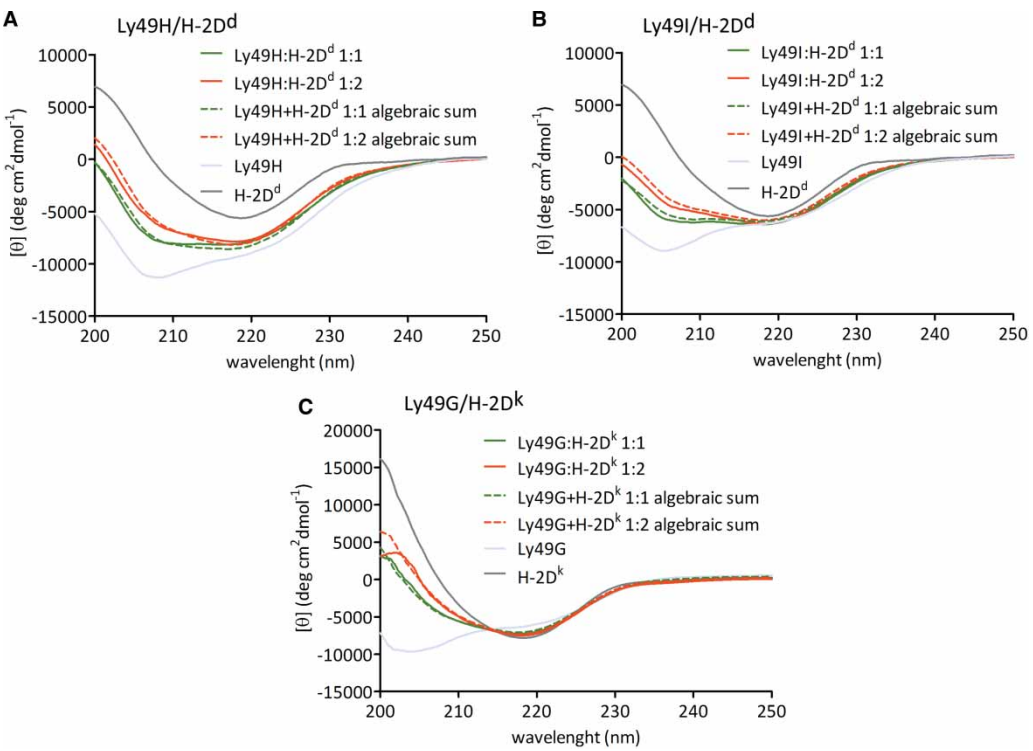

Figure 4. Far-UV CD spectra of Ly49H, Ly49I and Ly49G in combination with MHC-I.

Ly49H (**A**), Ly49I (**B**) and Ly49G (**C**) preincubated with MHC-I at molar ratios of 1:1 (*solid green lines*) and 1:2 (*solid red lines*) and the algebraic sum of spectra of Ly49 and one MHC-I molecule (*dashed green lines*) or of spectra of Ly49 and two MHC-I molecules (*dashed red lines*) are shown. *Light blue lines* for Ly49H (**A**), Ly49I (**B**) and Ly49G (**C**) spectra alone; *gray lines* for MHC-I spectra alone: $H\text{-}2D^d$ in (**A**) and in (**B**), and $H\text{-}2D^k$ in (**C**).

Biochemical Journal (2017) 474 179–194
DOI: 10.1042/BCJ20160876

protomer 1) and Ly49/MHC-I (MHC-I attached to protomer 2) are equivalent. The union of the first ligand to one of the monomers is equivalent to that of the second ligand to the other monomer. The molecular mechanism is represented by the following reaction scheme:

$$\begin{aligned} \text{Ly49} + \text{MHC-I} &\underset{\text{kd1}}{\overset{\text{ka1}}{\rightleftharpoons}} \text{Ly49/MHC-I} \\ \text{Ly49/MHC-I} + \text{MHC-I} &\underset{\text{kd2}}{\overset{\text{ka2}}{\rightleftharpoons}} \text{Ly49/(MHC-I)}_2 \end{aligned} \qquad \text{(Reaction Scheme I)}$$

where Ly49 can interchange between the backfolded and extended state, except in the final trimolecular complex, where a backfolded form of Ly49 is adopted.

For the sake of completeness, and to make the binding mechanism model choice more reliable, we compared the fitting of the proposed binding mechanism with the classical 1:1 Langmuir model and with the Ly49/m157 interaction-binding mechanism [20]. To decide which of the models is the most appropriate for our experimental data, we applied several statistical criteria, including the modified Akaike criterion (model selection criterion), Bayesian selection criterion (Bayesian information criterion), Hannan–Quinn information criterion and Zwanzig selection criterion to the available kinetic data. The equations of these statistics are provided in Supplementary Information and Supplementary Table S1 that indicates the statistic values obtained. According to this analysis, the above-proposed model (Reaction Scheme I) was found to be the most appropriate to describe the molecular interactions of Ly49/MHC-I.

To measure the kinetics underlying this mechanism, all sensograms for each Ly49H/MHC-I pair obtained at different temperatures were analyzed together and fitted globally according to the differential equations derived for the sequential binding model. Figure 5 shows sensograms for the Ly49H/H-2D^d, Ly49I/H-2D^d and Ly49G/H-2D^k pairs at temperatures of 5, 10, 15, 25 and 30°C with the fitted curves. The kinetic rate constants (association rate *ka* and dissociation rate *kd*) and macroscopic sequential equilibrium constants ($KA1 = ka1/kd1$ for the binding of the first H-2D and $KA2 = ka2/kd2$ for the binding of the second H-2D) are given in Tables 2 and 3. It is important to note that the macroscopic sequential constants $KA1$ and $KA2$ calculated ($KA = ka/kd$) from kinetic analysis of SPR data are consistent with the constants $Ks1$ and $Ks2$ determined by equilibrium solution FA assays. Both $KA1$ and $Ks1$ are $\sim 10^6\ M^{-1}$, and $KA2$ and $Ks2$ are $\sim 10^6\ M^{-1}$. This correspondence validates our results from different methods, integrating both kinetic and thermodynamic experiments into a coherent picture.

Activation energy analysis of Ly49/MHC-I interactions

To complete the study of Ly49 binding to MHC-I, we performed an Eyring analysis using the kinetic rate constants obtained from the SPR data. The dependence of these constants on temperature is plotted in Figure 6 for the Ly49H/H-2D^d, Ly49I/H-2D^d and Ly49G/H-2D^k pairs. The Eyring equation was fitted to the experimental points at the reference temperature of 25°C to render the activation parameters $\Delta H^0‡$ (activation enthalpy), $\Delta S^0‡$ (activation entropy) and $\Delta Cp^0‡$ (activation heat capacity) (Supplementary Table S2). The $\Delta G^0‡$ (activation free energy) was calculated directly from the kinetic rate constants.

Landscapes depicting the progression of the reaction at 25°C are shown for the free energy (Figure 7A), together with its deconvolution into enthalpic (Figure 7B) and entropic (Figure 7C) components for the Ly49H/H-2D^d, Ly49I/H-2D^d and Ly49G/H-2D^k interactions. Analysis of these landscapes established that the reactions are spontaneous and diffusion-controlled, where species encounter is the rate-limiting step. We reached this conclusion because the activation energy to form the complexes is ∼5 kcal/mol, based on the free energy landscapes. In contrast, the rate-limiting step for the Ly49/m157 interaction is a conformational change in Ly49 from the backfolded to the extended form, where the activation energy is much higher (15–30 kcal/mol) [20]. The binding of the first H-2D^d to Ly49H and to Ly49I depicts an entropic barrier compensated by a favorable enthalpic energy release. The binding of the second H-2D^d shows both enthalpic and entropic barriers. For the Ly49G/H-2D^k pair, however, binding of both the first and second H-2D^k ligand is characterized by entropic barriers to transition state formation, compensated by a favorable enthalpic energy release. Overall, the global thermodynamic parameters from the initial state (free forms of Ly49 and MHC-I) to the final state [Ly49/(MHC-I)$_2$ complex] are characterized by an enthalpic decrease in the system (exothermic reaction) together with an entropy increase, both contributing to a spontaneous interaction process.

Biochemical Journal (2017) **474** 179–194
DOI: 10.1042/BCJ20160876

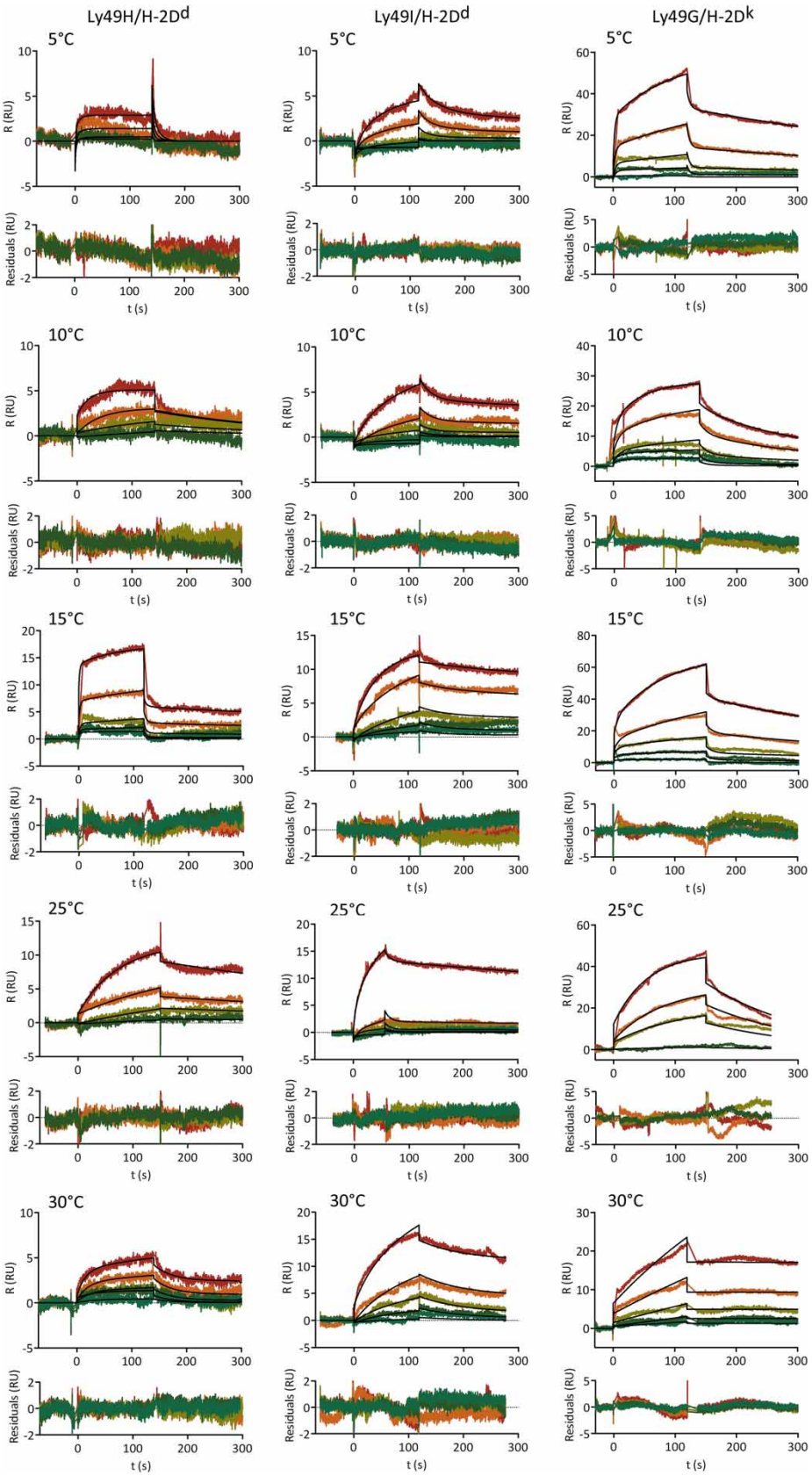

Figure 5. Sensograms for Ly49/MHC-I interactions at different temperatures.

Part 1 of 2

Biochemical Journal (2017) **474** 179–194
DOI: 10.1042/BCJ20160876

Figure 5. Sensograms for Ly49/MHC-I interactions at different temperatures. Part 2 of 2

Sensograms for Ly49H/H-2D^d ([H-2D^d] between 0.125 and 4 μM, half serial dilutions), for Ly49I/H-2D^d ([H-2D^d] between 0.156 and 5 μM, half serial dilutions) and for Ly49G/H-2D^k ([H-2D^k] between 0.23 and 15 μM, half serial dilutions) at 5, 10, 15, 25 and 30°C are shown. *Black lines* indicate the fitted curves using numerical integration with the BIAevaluation 4.1 software from the differential equations corresponding to the model considering sequential ligand binding. The kinetic rate constants and macroscopic sequential equilibrium constants are presented in Tables 2 and 3, respectively, for the Ly49H/H-2D^d, Ly49I/H-2D^d and Ly49G/H-2D^k pairs.

Table 2 Ly49H/H-2D^d, Ly49I/H-2D^d, Ly49G/H-2D^k and Ly49P/H-2D^k kinetic rate constants estimated from SPR kinetic analysis with the sequential ligand-binding model at different temperatures

T (°C)	*ka1* × 10^3 (M^{-1} s^{-1})	*kd1* × 10^{-3} (s^{-1})	*ka2* × 10^3 (M^{-1} s^{-1})	*kd2* × 10^{-3} (s^{-1})
Ly49H/H-2D^d				
5	20.4 ± 0.6	3.76 ± 0.07	500 ± 100	98 ± 7
10	8.0 ± 0.3	3.64 ± 0.09	2700 ± 100	700 ± 300
15	1.03 ± 0.03	0.08 ± 0.04	42 ± 2	0.076 ± 0.004
25	2.6 ± 0.1	0.9 ± 0.3	70 ± 20	1.5 ± 0.5
30	0.26 ± 0.04	0.64 ± 0.03	210 ± 90	300 ± 50
Ly49I/H-2D^d				
5	5.0 ± 0.3	42.6 ± 0.2	3.01 ± 0.08	1.75 ± 0.05
10	6.2 ± 0.3	53.4 ± 0.2	3.9 ± 0.1	1.98 ± 0.03
15	1.69 ± 0.01	0.649 ± 0.006	270 ± 40	436 ± 9
25	0.332 ± 0.002	1.13 ± 0.01	45 ± 8	59.3 ± 0.6
30	0.862 ± 0.005	4.87 ± 0.02	2.32 ± 0.04	0.28 ± 0.06
Ly49G/H-2D^k				
5	0.1641 ± 0.0006	1.590 ± 0.002	4.5 ± 0.3	12.84 ± 0.03
10	0.66 ± 0.01	2.64 ± 0.02	58 ± 4	80 ± 10
15	0.270 ± 0.003	2.80 ± 0.06	2.1 ± 0.2	3.2 ± 0.1
25	0.79 ± 0.03	6.5 ± 0.5	220 ± 30	41 ± 4
30	0.35 ± 0.01	0.57 ± 0.03	9 ± 2	3.7 ± 0.4
Ly49P/H-2D^k (MCMV peptide)				
10	140 ± 20	9.7 ± 0.9	450 ± 60	98 ± 7

Insensitivity of Ly49G to MHC-bound peptide

Deng et al. [17] proposed a structural classification of Ly49 receptors, differentiating two principal groups. In Group I Ly49s, recognition loop L3 of the NKD is interrupted by helix α3, as exemplified by Ly49C. Group I also includes Ly49H and Ly49I, among others. By comparison, Group II Ly49s, which include Ly49A, Ly49G and Ly49P, lack the α3 helix and display a continuous L3 loop [17]. Whereas Ly49C (Group I) binds MHC-I with different affinities depending on the sequence of the presented peptide [16], the binding of Ly49A (Group II) to MHC-I is not sensitive to peptide [7]. To test the prediction that MHC-I recognition by other Group II Ly49s is independent of the MHC-bound peptide [17], we conducted SPR assays for Ly49G binding to H-2D^k bearing two peptides of unrelated sequence: RRLGRTLLL from MT polyoma virus protein [22] and DRSLRLPAR from MCMV protein m107 (Figure 8) [23]. In agreement with the structure-based classification of Ly49 receptors [17], Ly49G engaged H-2D^k/MT and H-2D^k/MCMV with similar equilibrium binding constants for both the first and second MHC-I ligand, all on the order of 10^5 M^{-1}. This lack of peptide specificity would enable Ly49G and other Group II Ly49s to recognize MHC-I independently of the bound peptide, thereby enhancing the capacity of NK cells to efficiently monitor target cells for expression of MHC-I molecules that typically present thousands of different peptides [10].

Biochemical Journal (2017) **474** 179–194
DOI: 10.1042/BCJ20160876

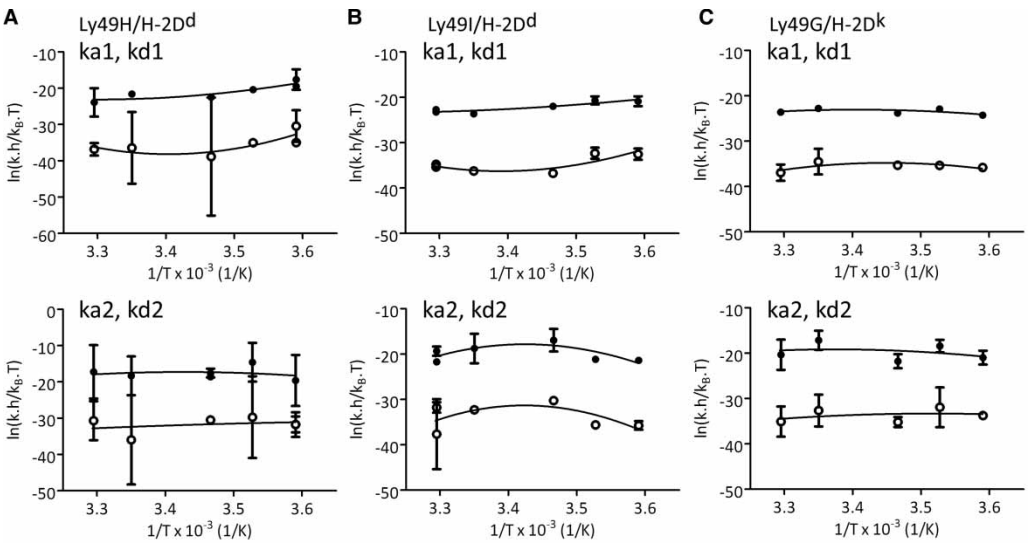

Figure 6. Eyring analysis using kinetic rate constants at different temperatures.

Eyring analysis using the kinetic rate constants obtained after applying the identical and independent binding site model to the SPR data for the Ly49H/H-2D^d (**A**), Ly49I/H-2D^d (**B**) and Ly49G/H-2D^k (**C**) interactions is shown. The Eyring equation was fitted to experimental data points at 25°C to obtain the thermodynamic activation parameters $\Delta H^0‡$, $\Delta S^0‡$ and $\Delta Cp^0‡$ (Supplementary Table S1). *Filled circles* indicate association data and *empty circles* indicate dissociation data. Error bars represent SD.

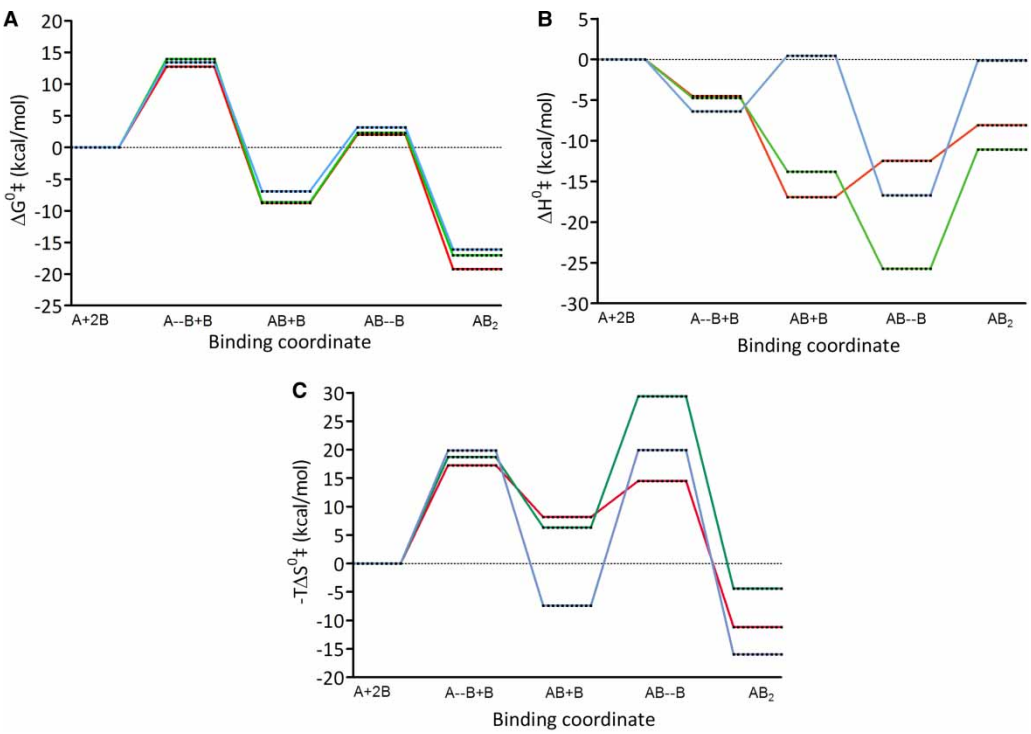

Figure 7. Reaction progress landscapes at 25°C.

Reaction progress landscapes at 25°C for the free energy (**A**) together with the deconvolution into enthalpic (**B**) and entropic (**C**) components for the Ly49H/H-2D^d (*red*), Ly49I/H-2D^d (*green*) and Ly49G/H-2D^k (*blue*) pairs are shown. *A*, Ly49; *B*, MHC-I; *A–B*, transition state for the binding to the first MHC-I; *AB*, Ly49 bound to one MHC-I molecule; *AB–B*, transition state for the binding to the second MHC-I; AB_2, Ly49 bound to two MHC-I molecules.

Biochemical Journal (2017) **474** 179–194
DOI: 10.1042/BCJ20160876

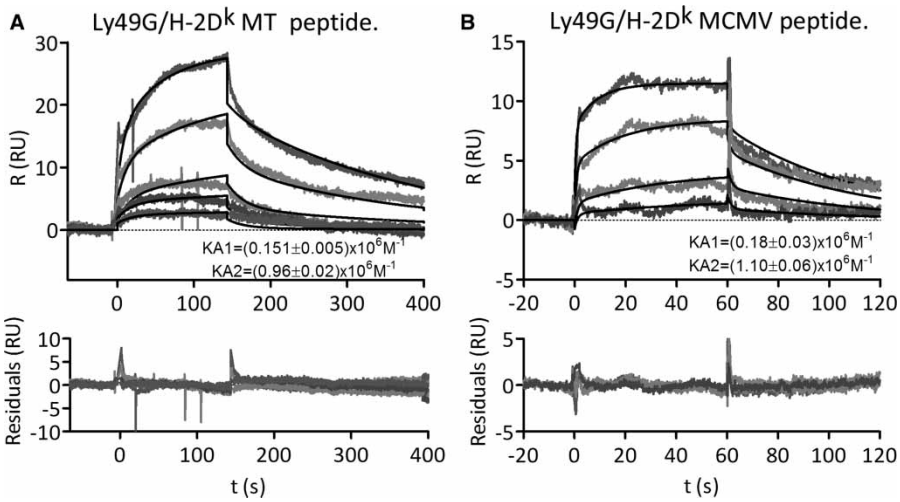

Figure 8. Interaction of Ly49G with H-2D^k bearing peptides of unrelated sequence at 10°C.

(**A**) Sensograms for the interaction of Ly49G with H-2D^k presenting a peptide (RRLGRTLLL) from MT polyoma virus protein [22]. H-2D^k molar concentrations were between 0.0146 and 15 μM. (**B**) Sensograms for the interaction of Ly49G with H-2D^k presenting a peptide (DRSLRLPAR) from MCMV protein m107 [23]. H-2D^k molar concentrations were between 2 and 8 μM. *Black lines* indicate the fitted curves using numerical integration with the BIAevaluation 4.1 software from the differential equations of the sequential ligand-binding model. The macroscopic sequential equilibrium constants are indicated. *R*, response.

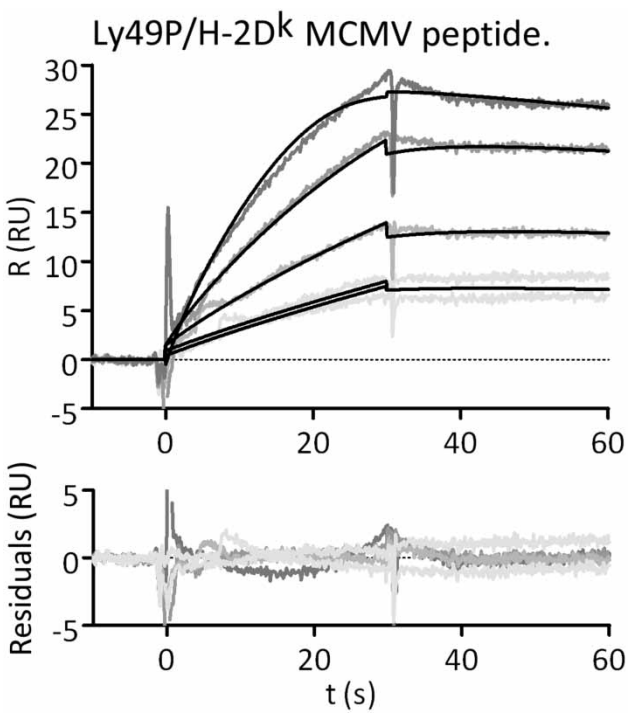

Figure 9. Activating Ly49 interactions with endogenous MHC-I at 10°C.

Sensograms for the interaction of Ly49P with H-2D^k bearing MCMV m107 peptide. The H-2D^k molar concentrations used were between 0.3 and 2.5 μM. *Black lines* indicate the fitted curves using numerical integration with the BIAevaluation 4.1 software of the differential equations corresponding to a model of sequential ligand binding. The kinetic rate constants and macroscopic sequential equilibrium constants are given in Tables 2 and 3. *R*, response.

Biochemical Journal (2017) **474** 179–194
DOI: 10.1042/BCJ20160876

Table 3 Ly49H/H-2D^d, Ly49I/H-2D^d, Ly49G/H-2D^k and Ly49P/H-2D^k binding equilibrium constants estimated from SPR kinetic analysis with the sequential ligand-binding model at different temperatures calculated as *KA* = *ka*/*kd*

T (°C)	*KA*1 × 10^6 (M^{-1})	*KA*2 × 10^6 (M^{-1})
Ly49H/H-2D^d		
5	5.4 ± 0.3	5 ± 2
10	2.2 ± 0.1	4 ± 3
15	12.7 ± 0.6	650 ± 60
25	2.8 ± 0.9	50 ± 30
30	0.41 ± 0.09	0.7 ± 0.4
Ly49I/H-2D^d		
5	0.12 ± 0.01	1.72 ± 0.09
10	0.12 ± 0.01	1.97 ± 0.08
15	2.60 ± 0.04	0.6 ± 0.1
25	0.24 ± 0.04	0.8 ± 0.1
30	0.177 ± 0.002	8 ± 2
Ly49G/H-2D^k		
5	0.1030 ± 0.0005	0.35 ± 0.03
10	0.249 ± 0.005	0.7 ± 0.2
15	0.096 ± 0.003	0.66 ± 0.07
25	0.12 ± 0.01	5 ± 1
30	0.62 ± 0.05	2.5 ± 0.6
Ly49P/H-2D^k (MCMV peptide)		
10	15 ± 3	5 ± 1

Activating versus inhibitory Ly49 receptors

Whereas Ly49I and Ly49G are inhibitory receptors, Ly49H and Ly49P are activating receptors. Sensograms of the Ly49P/H-2D^k interaction are shown in Figure 9. Kinetic rate constants (Table 2) and sequential equilibrium binding constants (Table 3) for activating Ly49s (Ly49H and Ly49P) are comparable with those for inhibitory Ly49s (Ly49I and Ly49G). Although kinetic rate constants (Table 2) and sequential equilibrium binding constants (Table 3) differ for each individual interaction pair because of the different amino acid residues involved in the interactions, constants for activating Ly49s (Ly49H and Ly49P) are comparable with those for inhibitory Ly49s (Ly49I and Ly49G). Kinetic rates and thermodynamic constants for activating and inhibitory Ly49s fall within defined ranges for the temperatures tested: ∼10^3–10^5 M^{-1} s^{-1} for *ka1* and *ka2* (Table 2); ∼10^{-2}–10^{-4} s^{-1} for *kd1* and *kd2* (Table 2); and ∼10^5–10^7 M^{-1} for *KA*1 and *KA*2 (Table 3). Variations do not depend on whether the Ly49s are activating or inhibitory, but are likely observed because several different Ly49 receptors are involved (Ly49H, Ly49I, Ly49G2 and Ly49P) that interact with different MHC-I alleles. Therefore, differences in signaling are not due to differences in the mechanism by which activating and inhibitory Ly49s bind MHC-I. Instead, signaling differences must be due to differences in the cytoplasmic domains of Ly49s, whereby inhibitory Ly49s transmit signals via ITIMs, whereas activating Ly49s instead use the noncovalently associated signaling homodimer DAP12, which contains ITAMs.

Discussion

In the present study, we analyzed the interaction of both inhibitory and activating Ly49 NK receptors with MHC-I ligands using SPR, fluorescence anisotropy and CD. The results allowed us to describe the binding mechanism and the activation energy parameters of Ly49/MHC-I interactions in fine detail. These experiments revealed major differences in the way Ly49 receptors engage MHC-I compared with the MCMV immunoevasin

Biochemical Journal (2017) **474** 179–194
DOI: 10.1042/BCJ20160876

m157 [20]. Moreover, these differences are readily understood in terms of the crystal structures of Ly49/MHC-I and Ly49/m157 complexes [7].

We showed previously that the Ly49/m157 interaction proceeds via a conformational selection mechanism where only the extended conformation of Ly49 is capable of binding the first m157 ligand, followed by binding of the second m157 ligand to form the Ly49/$(m157)_2$ trimolecular complex (Figure 1E) [20]. The interaction is characterized by strong positive co-operativity such that the second m157 binds the Ly49 homodimer with a 1000-fold higher sequential equilibrium constant than the first ($\sim 10^8$ versus $\sim 10^5\ M^{-1}$). This positive co-operativity is explained by a conformational transition in Ly49 from its backfolded to extended form upon binding m157. The transition is required because, in the structure of the Ly49/m157 complex, m157 binds to the stalk region of Ly49, rather than to the NKDs, which recognize MHC-I [19]. The Ly49/m157 interaction is only possible with Ly49 in the extended state (Figure 1B), since the stalk region is not accessible to m157 in the backfolded state due to its intimate association with the NKDs (Figure 1A).

In sharp contrast with the Ly49/m157 interaction, we found that the interaction of four different Ly49 receptors (Ly49G, Ly49H, Ly49I and Ly49P) with two different MHC-I ligands (H-2D^d and H-2D^k) presenting three different peptides (HIV, MT and MCMV) is not positively co-operative at the same level as it is for Ly49/m157. This feature is likely to apply to other Ly49/MHC-I interaction pairs. Rather, the two MHC-I binding sites of the Ly49 homodimer may present a slightly positive co-operativity process when binding the second MHC-I ligand, as demonstrated by both thermodynamic and kinetic analyses. In particular, FA equilibrium measurements gave almost similar microscopic binding constants (k' and k) for the two sites ($\sim 10^6\ M^{-1}$). This result is entirely consistent with the crystal structure of the Ly49C/H-2K^b complex [16,17], in which the Ly49C homodimer binds H-2K^b bivalently, with each NKD of the Ly49 dimer making identical contacts with MHC-I (Figure 1C).

Whereas the Ly49/m157 interaction is accompanied by a requisite conformational transition in Ly49 from the backfolded to extended state [20], far-UV CD analysis revealed no indication of such a transition for Ly49/MHC-I interactions. This finding is in agreement with structural results showing that MHC-I, unlike m157, can engage Ly49s in the backfolded conformation, which mediates *trans* recognition of MHC-I (Figure 1C) [18]. Since unbound Ly49 receptors exist predominantly in the more stable backfolded state [18], no major structural change would be required for MHC-I binding. Moreover, the less stable extended state is also compatible with MHC-I recognition, albeit in *cis* (Figure 1D).

To determine whether Ly49/MHC-I reactions were diffusion-controlled or activation-controlled, kinetic association rates and $\Delta H^0‡$ values were considered [34]. Although *ka1* and *ka2* values (*ka1* $\sim 10^3\ M^{-1}\ s^{-1}$ and *ka2* $\sim 10^4\ M^{-1}\ s^{-1}$) were 1 to 2 orders of magnitude lower than typically reported *ka* values for diffusion-controlled mechanisms ($\sim 10^5\ M^{-1}\ s^{-1}$) [35], $\Delta H^0‡$ values were between 4 and −15 kcal/mol, which are of the same order as those reported for diffusion-limited interactions in water (4–5 kcal/mol) [36]. Despite the low rate constants, we conclude that Ly49/MHC-I interactions are diffusion-controlled because of the $\Delta H^0‡$ values, and because CD spectra provided no evidence for conformational changes upon complex formation.

According to kinetic data, dissociation of the trimolecular complex Ly49/$(MHC\text{-}I)_2$ appears to occur more rapidly than that of the bimolecular complex Ly49/MHC-I. The higher dissociation rate constant for the second stage of the interaction mechanism could enable Ly49s to quickly release MHC-I molecules on a juxtaposed target cell bound in *trans* in order to permit the NK cell to probe other target cells for surface expression of MHC-I (Figure 1C). In addition, rapid dissociation of the Ly49/$(MHC\text{-}I)_2$ complex at the NK cell–target cell interface would facilitate formation of *cis* interactions with MHC-I molecules on the same NK cell (Figure 1D), which increases the sensitivity of NK cells to diseased cells by lowering the threshold at which NK cell activation exceeds inhibition [18,37].

Ly49H/H-2D^d, Ly49I/H-2D^d and Ly49G-H-2D^k reaction progress landscapes revealed significant differences in activation energy parameters. Binding of the first H-2D^d ligand to Ly49H and Ly49I features an entropic barrier compensated by a favorable enthalpy, whereas binding of the second H-2D^d ligand shows enthalpic and entropic barriers. For the Ly49G/H-2D^k pair, in contrast, binding of both the first and second H-2D^k ligand is characterized by entropic barriers, compensated by favorable enthalpies. These thermodynamic differences, along with the slightly positive co-operativity process shown for Ly49H and Ly49I, but not for Ly49G, may reflect structural differences between Ly49H and Ly49I on the one hand, both of which are classified as Group I Ly49s based on the NKD structure, versus Ly49G on the other hand, which belongs to Group II [17].

Ly49/MHC-I and Ly49/m157 interactions differ markedly in terms of their dissociation rate constants. Thus, dissociation of the second m157 ligand from the Ly49 homodimer [20] is slower than dissociation of either

MHC-I ligand from Ly49 (10^{-3}–10^{-4} s^{-1} for Ly49/m157 versus 10^{-2} s^{-1} for Ly49/MHC-I). The longer half-life of Ly49/$(m157)_2$ complexes (~150–350 s) may be required to compensate for the relatively low number of m157 molecules expressed on MCMV-infected cells, thereby assuring delivery of a sufficiently strong inhibitory signal to the NK cell that prevents lysis of the infected cell and enables the virus to survive. In this way, m157 has evolved into a potent MCMV immunoevasin. In contrast, the shorter half-life of Ly49/$(MHC\text{-}I)_2$ complexes (~10–20 s) that we observed here may suffice for effective signal transmission, given the high levels of MHC-I molecules typically expressed on normal cells. In addition, fast dissociation of Ly49/$(MHC\text{-}I)_2$ complexes would permit an NK cell to easily disengage itself from an encounter with a particular target cell, so that it can quickly move on to screen other cells for MHC-I expression. Therefore, the distinct kinetics of Ly49/MHC-I and Ly49/m157 interactions reflect the opposing roles of NK cells to rapidly scan for virally infected cells with reduced MHC-I expression, and of viruses to escape detection and elimination by NK cells using immunoevasins such as m157.

Abbreviations

CD, circular dichroism; FA, fluorescence anisotropy; FITC, fluorescein isothiocyanate; HIV, human immunodeficiency virus; ITAMs, immunoreceptor tyrosine-based activating motifs; ITIMs, immunoreceptor tyrosine-based inhibitory motifs; KIRs, killer immunoglobulin-like receptors; Ly49H, activating Ly49; Ly49I, inhibitory Ly49; MCMV, mouse cytomegalovirus; MT, middle T; NK, natural killer; NKD, natural killer receptor domain; RU, response unit; SPR, surface plasmon resonance.

Author Contribution

P.N.R., M.B.S., S.N.T., M.B.A., M.J.F.L., M.M.F. and E.L.M. cloned and produced the recombinant molecules, designed and conducted SPR experiments, and analyzed the results. P.N.R., L.M.C. and J.M.D. designed and conducted FA binding assays and far-UV CD experiments. R.A.M., M.M.F. and E.L.M. conceived the idea for the project and wrote the paper with P.N.R.

Funding

This work was supported by the University of Buenos Aires, the National Research Council of Argentina (CONICET) and Agencia Nacional de Promoción Científica y Tecnológica grants [PICT-2010-373 to M.M.F.], [PICT-2007-0632 and PICT-2011-0861 to J.M.D.], [PICT-2010-0460 to L.M.C.] and [PICT-2008-1139 and PICT-2013-2328 to E.L.M.]. E.L.M. is also supported by the Fogarty International Center [TW007972] and International Centre for Genetic Engineering and Biotechnology [CRP/ARG09-02]. R.A.M. is supported by National Institutes of Health grant [AI47990]. The funders had no role in the study design, data collection and analysis, decision to publish or preparation of the manuscript.

Acknowledgements

We are grateful to S.K. Anderson (National Cancer Institute) and A.P. Makrigiannis (Clinical Research Institute of Montreal) for providing Ly49 cDNAs.

Competing Interests

The Authors declare that there are no competing interests associated with the manuscript.

References

1 Di Santo, J.P. (2008) Natural killer cells: diversity in search of a niche. *Nat. Immunol.* **9**, 473–475 doi:10.1038/ni.f.201
2 Vivier, E., Tomasello, E., Baratin, M., Walzer, T. and Ugolini, S. (2008) Functions of natural killer cells. *Nat. Immunol.* **9**, 503–510 doi:10.1038/ni1582
3 Bryceson, Y.T., Chiang, S.C.C., Darmanin, S., Fauriat, C., Schlums, H., Theorell, J. et al. (2011) Molecular mechanisms of natural killer cell activation. *J. Innate Immun.* **3**, 216–226 doi:10.1159/000325265
4 Vivier, E., Raulet, D.H., Moretta, A., Caligiuri, M.A., Zitvogel, L., Lanier, L.L. et al. (2011) Innate or adaptive immunity? The example of natural killer cells. *Science* **331**, 44–49 doi:10.1126/science.1198687
5 Lanier, L.L. (2008) Evolutionary struggles between NK cells and viruses. *Nat. Rev. Immunol.* **8**, 259–268 doi:10.1038/nri2276
6 Long, E.O., Kim, H.S., Liu, D., Peterson, M.E. and Rajagopalan, S. (2013) Controlling natural killer cell responses: integration of signals for activation and inhibition. *Annu. Rev. Immunol.* **31**, 227–258 doi:10.1146/annurev-immunol-020711-075005
7 Li, Y. and Mariuzza, R.A. (2014) Structural basis for recognition of cellular and viral ligands by NK cell receptors. *Front. Immunol.* **5**, 123 doi:10.3389/fimmu.2014.00123
8 Anderson, S.K., Ortaldo, J.R. and McVicar, D.W. (2001) The ever-expanding Ly49 gene family: repertoire and signaling. *Immunol. Rev.* **181**, 79–89 doi:10.1034/j.1600-065X.2001.1810106.x

Biochemical Journal (2017) **474** 179–194
DOI: 10.1042/BCJ20160876

9 Yokoyama, W.M. and Plougastel, B.F.M. (2003) Immune functions encoded by the natural killer gene complex. *Nat. Rev. Immunol.* **3**, 304–316 doi:10.1038/nri1055
10 Lanier, L.L. (2005) NK cell recognition. *Annu. Rev. Immunol.* **23**, 225–274 doi:10.1146/annurev.immunol.23.021704.115526
11 Arase, H., Mocarski, E.S., Campbell, A.E., Hill, A.B. and Lanier, L.L. (2002) Direct recognition of cytomegalovirus by activating and inhibitory NK cell receptors. *Science* **296**, 1323–1326 doi:10.1126/science.1070884
12 Smith, H.R.C., Heusel, J.W., Mehta, I.K., Kim, S., Dorner, B.G., Naidenko, O.V. et al. (2002) Recognition of a virus-encoded ligand by a natural killer cell activation receptor. *Proc. Natl Acad. Sci. U.S.A.* **99**, 8826–8831 doi:10.1073/pnas.092258599
13 Lanier, L.L. (2008) Up on the tightrope: natural killer cell activation and inhibition. *Nat. Immunol.* **9**, 495–502 doi:10.1038/ni1581
14 Corbett, A.J., Coudert, J.D., Forbes, C.A. and Scalzo, A.A. (2011) Functional consequences of natural sequence variation of murine cytomegalovirus m157 for Ly49 receptor specificity and NK cell activation. *J. Immunol.* **186**, 1713–1722 doi:10.4049/jimmunol.1003308
15 Tormo, J., Natarajan, K., Margulies, D.H. and Mariuzza, R.A. (1999) Crystal structure of a lectin-like natural killer cell receptor bound to its MHC class I ligand. *Nature* **402**, 623–631 doi:10.1038/45170
16 Dam, J., Guan, R., Natarajan, K., Dimasi, N., Chlewicki, L.K., Kranz, D.M. et al. (2003) Variable MHC class I engagement by Ly49 natural killer cell receptors demonstrated by the crystal structure of Ly49C bound to H-2Kb. *Nat. Immunol.* **4**, 1213–1222 doi:10.1038/ni1006
17 Deng, L., Cho, S., Malchiodi, E.L., Kerzic, M.C., Dam, J. and Mariuzza, R.A. (2008) Molecular architecture of the major histocompatibility complex class I-binding site of Ly49 natural killer cell receptors. *J. Biol. Chem.* **283**, 16840–16849 doi:10.1074/jbc.M801526200
18 Back, J., Malchiodi, E.L., Cho, S., Scarpellino, L., Schneider, P., Kerzic, M.C. et al. (2009) Distinct conformations of Ly49 natural killer cell receptors mediate MHC class I recognition in *trans* and *cis*. *Immunity* **31**, 598–608 doi:10.1016/j.immuni.2009.07.007
19 Berry, R., Ng, N., Saunders, P.M., Vivian, J.P., Lin, J., Deuss, F.A. et al. (2013) Targeting of a natural killer cell receptor family by a viral immunoevasin. *Nat. Immunol.* **14**, 699–705 doi:10.1038/ni.2605
20 Romasanta, P.R., Curto, L.M., Urtasun, N., Sarratea, M.B., Chiappini, S.A., Miranda, M.V. et al. (2014) A positive cooperativity binding model between Ly49 natural killer cell receptors and the viral immunoevasin m157: kinetic and thermodynamic studies. *J. Biol. Chem.* **289**, 5083–5096 doi:10.1074/jbc.M113.532929
21 Li, H., Natarajan, K., Malchiodi, E.L., Margulies, D.H. and Mariuzza, R.A. (1998) Three-dimensional structure of H-2Dd complexed with an immunodominant peptide from human immunodeficiency virus envelope glycoprotein 120. *J. Mol. Biol.* **283**, 179–191 doi:10.1006/jmbi.1998.2091
22 Lukacher, A.E. and Wilson, C.S. (1998) Resistance to polyoma virus-induced tumors correlates with CTL recognition of an immunodominant H-2Dk-restricted epitope in the middle T protein. *J. Immunol.* **160**, 1724–1734 PMID:9469430
23 Kattenhorn, L.M., Mills, R., Wagner, M., Lomsadze, A., Makeev, V., Borodovsky, M. et al. (2004) Identification of proteins associated with murine cytomegalovirus virions. *J. Virol.* **78**, 11187–11197 doi:10.1128/JVI.78.20.11187-11197.2004
24 Buus, S., Lauemøller, S.L., Worning, P., Kesmir, C., Frimurer, T., Corbet, S. et al. (2003) Sensitive quantitative predictions of peptide-MHC binding by a 'Query by Committee' artificial neural network approach. *Tissue Antigens* **62**, 378–384 doi:10.1034/j.1399-0039.2003.00112.x
25 Hill, A.V. (1910) The possible effects of the aggregation of the molecules of hemoglobin on its dissociation curves. *J. Physiol.* **40**, 4–7
26 Morton, T.A., Myszka, D.G. and Chaiken, I.M. (1995) Interpreting complex binding kinetics from optical biosensors: a comparison of analysis by linearization, the integrated rate equation, and numerical integration. *Anal. Biochem.* **227**, 176–185 doi:10.1006/abio.1995.1268
27 Myszka, D.G., Morton, T.A., Doyle, M.L. and Chaiken, I.M. (1997) Kinetic analysis of a protein antigen-antibody interaction limited by mass transport on an optical biosensor. *Biophys. Chem.* **64**, 127–137 doi:10.1016/S0301-4622(96)02230-2
28 Press, W.H., Teukolsky, S.A., Vetterling, W.T. and Flannery, B.P. (1999) *Numerical Recipes in C*, 2nd edn, pp. 801–806, Cambridge University Press, Cambridge, U.K.
29 Gutfreund, H. (1995) *Kinetics for the Life Sciences: Receptors, Transmitters and Catalysts*, pp. 236–247, Cambridge University Press, Cambridge, U.K.
30 Hill, T.L. (1985) *Cooperativity Theory in Biochemistry: Steady-State and Equilibrium Systems*, pp. 59–87, Springer-Verlag, New York
31 Cantor, C.R. and Schimmel, P.R. (1980) *Biophysical Chemistry: Parts I–III*, pp. 849–886, W. H. Freeman, San Francisco
32 Wyman, J. and Gill, S.J. (1990) *Binding and Linkage: Functional Chemistry of Biological Macromolecules*, University Science Books, Mill Valley, CA
33 Weber, G. (1992) Protein interactions, pp. 1–287, Chapman and Hall, New York
34 Schreiber, G. (2002) Kinetic studies of protein-protein interactions. *Curr. Opin. Struct. Biol.* **12**, 41–47 doi:10.1016/S0959-440X(02)00287-7
35 De La Cruz, E.M. and Pollard, T.D. (1995) Nucleotide-free actin: stabilization by sucrose and nucleotide binding kinetics. *Biochemistry* **34**, 5452–5461 doi:10.1021/bi00016a016
36 Lohman, T.M. (1986) Kinetics of protein-nucleic acid interactions: use of salt effects to probe mechanisms of interaction. *CRC Crit. Rev. Biochem.* **19**, 191–245 doi:10.3109/10409238609084656
37 Doucey, M.-A., Scarpellino, L., Zimmer, J., Guillaume, P., Luescher, I.F., Bron, C. et al. (2004) *Cis* association of Ly49A with MHC class I restricts natural killer cell inhibition. *Nat. Immunol.* **5**, 328–336 doi:10.1038/ni1043